Radboud Repository

Radboud University Nijmegen

PDF hosted at the Radboud Repository of the Radboud University Nijmegen

The following full text is a preprint version which may differ from the publisher's version.

For additional information about this publication click this link.
http://hdl.handle.net/2066/104017

Please be advised that this information was generated on 2017-12-06 and may be subject to change.

Nonlinear dynamics of dimers on periodic substrates

C. Fusco*, A. Fasolino and T. Janssen

Department of Theoretical Physics, University of Nijmegen, Toernooiveld 1, 6525 ED Nijmegen, The Netherlands

We study the dynamics of a dimer moving on a periodic one-dimensional substrate as a function of the initial kinetic energy at zero temperature. The aim is to describe, in a simplified picture, the microscopic dynamics of diatomic molecules on periodic surfaces, which is of importance for thin film formation and crystal growth. We find a complex behaviour, characterized by a variety of dynamical regimes, namely oscillatory, "quasi-diffusive" (chaotic) and drift motion. Parametrically resonant excitations of internal vibrations can be induced both by oscillatory and drift motion of the centre of mass. For weakly bound dimers a chaotic regime is found for a whole range of velocities between two non-chaotic phases at low and high kinetic energy. The chaotic features have been monitored by studying the Lyapunov exponents and the power spectra. Moreover, for a short-range interaction, the dimer can dissociate due to the parametric excitation of the internal motion.

68.35.Ja, 05.45.-a, 47.52.+j

I. INTRODUCTION

Thin-film growth is a topic of great importance both from the theoretical and experimental point of view [1]. In order to build a microscopic theory of crystal growth, it is fundamental to understand isolated-adatom surface diffusion, and indeed a great amount of work has been devoted to the monomer case during the last decades [2–6]. Once individual atoms are adsorbed on a surface, they can meet each other thus forming dimers. In spite of this very simple morphology, dimers display a peculiar and intriguing diffusive behaviour [7–14]. In this paper we show that the strong nonlinearities arising during the motion of dimers on a periodic substrate make dimer dynamics a very complex phenomenon. Here, we study the problem of a one-dimensional dimer moving on a rigid periodic substrate at $T = 0$. A one-dimensional model is relevant since one-dimensional dimer diffusion occurs in real systems, in particular along steps and on channeled (110) metal surfaces [15]. Although some aspects of dimer energetics and dynamics have been recently considered (see in particular Refs. [8,9,11]), here we focus on the nonlinear microscopic dynamics of this model, which gives rise to different regimes depending on the initial velocity and on the strength of the dimer interaction. In particular, chaotic motion with long jumps is found between the oscillatory behaviour at low initial kinetic energy and the drift motion at high initial kinetic energy. In all these regimes, situations can be found where the centre of mass (CM) motion drives excitations of the dimer vibrations which can lead to dissociation for short range interatomic interactions. Such a complexity in the dynamical behaviour at $T = 0$ is relevant to understand the thermal diffusion problem. In particular, the chaotic behaviour which dominates for weakly bound dimers can account for the non-trivial dependence of the diffusion constant on the strength of the interatomic interaction reported in Ref. [9].

Chaotic motion can occur in nonlinear systems with at least three variables. Much studied is the case of systems characterized by a single spatial coordinate subjected to an external drive [16–20]. Besides, a system of interacting particles can exhibit chaotic motion with "quasi-diffusive" features in one dimension [21–23]. This can happen even without the presence of an external drive, as we will show below. In view of the sinusoidal potential and of the phase space dimension, our model bears some resemblance to an undriven double pendulum [24–26]. However, in our case, the possibility to perform either oscillatory or drift motion leads to the appearance and subsequent disappearance of chaos for increasing initial kinetic energy.

In Sect. II we describe our model. Sect. III is devoted to the discussion of the linearized version of the system, in which a semi-analytical treatment can be performed. Sect. IV analyses the dynamics of the full system, and in Sect. V we discuss the chaotic properties of the system. Some concluding remarks are presented in Sect. VI.

II. MODEL

We consider a dimer moving on a periodic one-dimensional substrate at zero temperature without damping. The particle-substrate interaction is modelled by a periodic function U:

$$U(x_1, x_2) = U_0(2 - \cos(kx_1) - \cos(kx_2)) \qquad (1)$$

---

where x_i represents the spatial coordinate of particle i ($i = 1, 2$), $2U_0$ is the potential barrier per particle and $k = 2\pi/a$, a being the substrate lattice constant. Most of the results presented here have been obtained using a harmonic interatomic potential:

$$V(x_1, x_2) = \frac{K}{2}(x_2 - x_1 - l)^2, \qquad (2)$$

where K is the force constant and l is the spring equilibrium length. We also used short range interatomic interactions, such as the Lennard-Jones (LJ) potential (see Sect. IV B).

The equations of motion are:

$$\begin{cases} m\ddot{x}_1 = K(x_2 - x_1 - l) - kU_0\sin(kx_1) \\ m\ddot{x}_2 = K(x_1 - x_2 + l) - kU_0\sin(kx_2) \end{cases} \qquad (3)$$

where m is the mass of each particle. We rescale the variables in the following way:

$$\tilde{x}_i = kx_i, \quad \tilde{t} = t/\tau, \quad \tilde{U}_0 = U_0/E_T, \quad \tilde{l} = kl, \quad \tilde{K} = K/(E_T k^2)$$

where E_T is a reference energy and $\tau = [m/(E_T k^2)]^{1/2}$. In these units the equations of motion become (in the following we will omit the tildes for simplicity)

$$\begin{cases} \ddot{x}_1 = K(x_2 - x_1 - l) - U_0\sin x_1 \\ \ddot{x}_2 = K(x_1 - x_2 + l) - U_0\sin x_2 \end{cases} \qquad (4)$$

In the CM and relative coordinates frame we have

$$\begin{cases} \ddot{x}_{CM} = -U_0\sin x_{CM}\cos(x_r/2 + l/2) \\ \ddot{x}_r = -2Kx_r - 2U_0\cos x_{CM}\sin(x_r/2 + l/2) \end{cases} \qquad (5)$$

where $x_{CM} = (x_1 + x_2)/2$ is the CM coordinate and $x_r = x_2 - x_1 - l$ is the relative coordinate. We concentrate on the commensurate case in which $l = a = 2\pi$, i.e. the spring natural length is equal to the period of the substrate potential. In this situation the minimum energy configuration does not depend on K (namely $x_1 = 0$ and $x_2 = a$ minimize the total potential energy) and moreover a linearization around $x_r = 0$ offers the possibility to treat the problem in a semi-analytical way. This has the advantage to give a closer insight on the dynamical features of this system.

We perform molecular dynamics simulations, integrating the equations of motion (4) using a velocity-Verlet algorithm, with time step $\Delta = 10^{-4}$.

III. DYNAMICS OF THE LINEARIZED SYSTEM

When $x_r \simeq 0$, as at the beginning of the motion starting from equilibrium, we can linearize in x_r the equations of motion (5):

$$\ddot{x}_{CM} \simeq U_0\sin x_{CM} \qquad (6a)$$

$$\ddot{x}_r \simeq -2K(1 - \frac{U_0}{2K}\cos x_{CM})x_r. \qquad (6b)$$

As initial conditions we choose

$$x_{CM}(0) = x_0 = a/2 \quad \dot{x}_{CM}(0) = v_0$$
$$x_r(0) = 0 \qquad\qquad \dot{x}_r(0) = 0.$$

In this way we give an initial kinetic energy to the dimer at equilibrium (alternatively one could have chosen to give an initial potential energy, i.e. $\dot{x}_{CM}(0) = 0$ and $x_{CM}(0) \neq a/2$). The minimum kinetic energy for the CM to get out of the potential is $v_0^2 = 4U_0$ if $v_1 = v_2 = v_0$ (v_i is the initial velocity of particle i). Below this threshold value (namely $v_0 < \sqrt{4U_0}$) Eq. (6a) coincides with that of a classical pendulum for which the amplitude as a function of the period of oscillation is known in terms of an elliptic integral [27], as shown in Fig. 1(a).
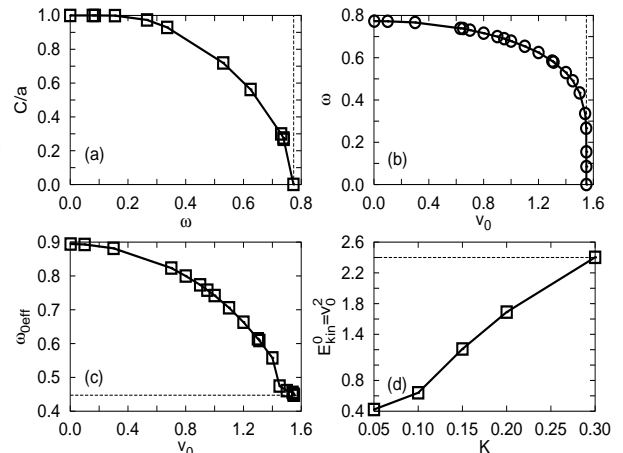

FIG. 1. Relation between amplitude and frequency of oscillation as given by the solution of Eq. 6a (a), between CM frequency of oscillation and CM initial velocity (b) and between the effective stretching frequency and CM initial velocity (c), obtained by numerical calculations for $U_0 = 0.6$ (solid lines). The lower borders of instability regions as a function of K are plotted in (d). The vertical dashed lines in (a) and in (b) indicate respectively the frequency of small oscillations $\sqrt{U_0} = 0.774$ and the velocity corresponding to the threshold for drift motion $\sqrt{4U_0} = 1.5492$. The horizontal dashed lines in (c) and (d) correspond respectively to $\omega_{0eff} = \sqrt{2K}$ ($K = 0.1$), which is reached when $v_0 \geq \sqrt{4U_0}$, and to the energy threshold for drift motion $\sqrt{4U_0}$.

The maximum amplitude of oscillation of the CM is determined by v_0. In this case

$$x_{CM} \simeq x_0 + \frac{C}{2}\sin(\omega t). \qquad (7)$$

with $\omega = \omega(v_0)$ (see Fig. 1(b)). This means that

$$\cos x_{CM} \simeq A + B\cos(2\omega t) \qquad (8)$$

with A and B depending on v_0 via ω. Inserting (8) into the equation of motion for x_r (6b) we obtain the equation of a parametric oscillator:

$$\ddot{x}_r = -\omega_{0eff}^2(1 + h\cos(2\omega t))x_r \qquad (9)$$

2

where $\omega_{0eff} \equiv \sqrt{2K - AU_0}$ and $h \equiv BU_0/\omega_{0eff}^2$. It is worth noting that the stretching frequency of the free dimer $\sqrt{2K}$ becomes $\sqrt{2K + U_0}$ in the external potential (this is true when the CM is fixed at the equilibrium position). But in Eq. (6a) the motion of x_r is further affected by the oscillatory behaviour of the CM and its natural frequency changes into $\omega_{0eff} \equiv \sqrt{2K - AU_0}$. Conversely, when $v_0 > \sqrt{4U_0}$ the CM performs a drift motion, i.e.

$$x_{CM} \simeq x_0 + <v_{CM}> t, \qquad (10)$$

where $< \cdot >$ denotes time averages and $<v_{CM}>$ is the drift CM velocity. By defining ω as $\omega = <v_{CM}>/2$ the equation for x_r remains in the form (9) with $\omega_{0eff} \equiv \sqrt{2K}$ and $h \equiv U_0/(2K)$ (i.e. $A = 0$ and $B = 1$).

The CM motion (either oscillatory or drifting), as considered in the linearized Eq. (6a), drives parametrically the internal motion of the dimer. We establish the instability ranges by monitoring for which values of the initial velocity v_0 an exponential increase of x_r is found. The relation between the initial velocity v_0 and the frequency ω_{0eff} is shown in Fig. 1(c) for several values of $v_0 < \sqrt{4U_0}$. In order to understand the energy threshold for the excitation of parametric resonances, we plot the lower borders of the instability regions as a function of K in Fig. 1(d) when the total initial kinetic energy $E_{kin}^0 = v_0^2$ is less than the potential barrier $4U_0$. In this way we can identify a critical value $K = K_c$ above which the parametric resonance can be excited only if the CM performs a drift motion (e.g. $E_{kin}^0 > 4U_0$). It turns out that $K_c \simeq 0.3$ for $U_0 = 0.6$. Since ω_{0eff} is determined by K, by considering different values of K we can construct the standard picture for parametric instabilities relating h to ω. One can recognize the main resonance for $\omega = \omega_{0eff}$ (Fig. 2). The boundaries of the region of instability are given by the stars in Fig. 2.
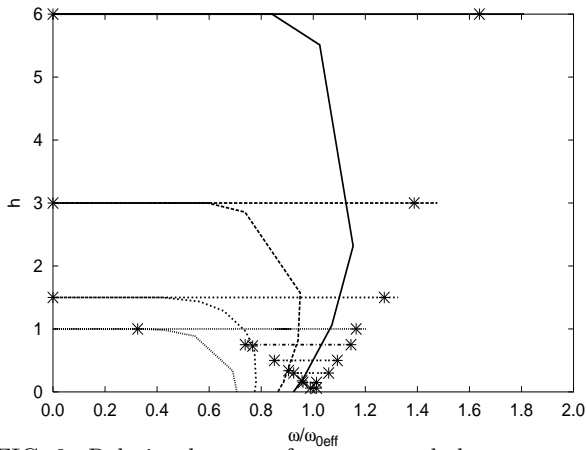

FIG. 2. Relation between frequency and the parameter h of Eq. (9) for different values of K (from top to bottom: $K = 0.05, 0.1, 0.2, 0.3, 0.4, 0.6, 1, 2, 5$) and $U_0 = 0.6$. The region in which the parametric resonance occurs is bounded by the stars.

The different curves represent h as a function of ω for different values of K. Note that, at fixed K, h increases when ω decreases (e.g. when the amplitude of oscillation increases and $v_0 < \sqrt{4U_0}$), but when the CM overcomes the barrier, h reaches the constant value $U_0/(2K)$. Moreover, the range of frequency in which instability is observed is larger for smaller values of K. An example of parametric resonance is shown in Fig. 3(a): x_r oscillates and its amplitude increases exponentially. In Fig. 3(b) a blow up of the behaviour of x_r and of the drive x_{CM}, oscillating at the same frequency, is also shown.

IV. DYNAMICS OF THE FULL SYSTEM

A. Harmonic case

Now we consider the original system of equations of motion Eq. (5). The linearization given by Eq. (6a) allows to understand some of the dynamical features of the full system. However, the CM and relative motion equations are coupled and this results in a qualitatively different behaviour with respect to the simple approximation discussed in Sect. III. In particular, we note that the feedback of x_r on x_{CM} drives the CM out of the instability window found for the linearized system Eq. (9).
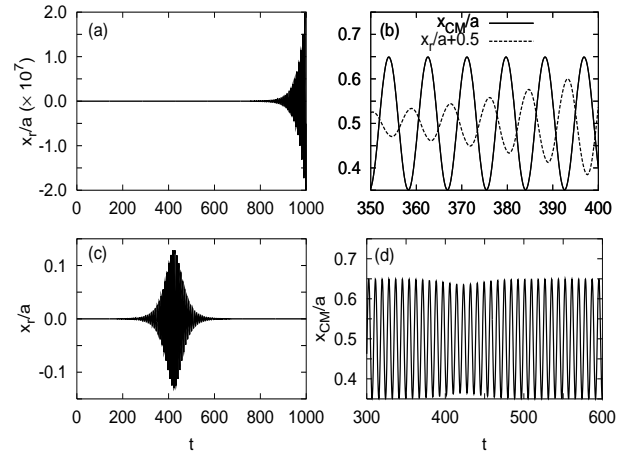

FIG. 3. Comparison between relative and CM motion of the linearized system Eq. (6a) (upper panel) and those obtained by integrating the complete system Eq. (4) (lower panel). The relative motion plotted in (a) is the numerical result of the integration of Eq. (9). The CM and relative coordinate of the linearized equations, which are plotted in (b), oscillate with the same frequency. The CM of the full system is shown in (d) where we note a decrease of amplitude at the point in which the relative motion starts to decrease in (c). Only the envelope of the rapid oscillations of x_r is visible on the left panel ((a) and (c)). The parameters used in the simulation are $U_0 = 0.6$, $K = 0.05$ and $v_0 = 0.7$. All lengths are rescaled to the substrate lattice constant a.

An example is illustrated in Fig. 3, where we compare the motion of the complete and of the linearized system. As we can see in Fig. 3(c), the parametric increase of x_r found for the linearized equations is followed by a decrease, due to the fact that the feedback of x_r on x_{CM} causes a change of the amplitude of the CM at that point ($t \simeq 400$ in Fig. 3(d)). However, when x_r decreases, the instability reappears and the relative motion increases again (although it is not shown in the figure). The system gets in and out the instability window, because we are considering a case that is almost at the border. Instead, in Fig. 4 we show a case which is in the centre of the region of instability: we can note that after an initial transient the relative motion is always excited, and its behaviour is more irregular so that it is not possible to identify a clear unique frequency of oscillation and a unique rate of increase. This behaviour is caused by the shift in position inside the instability window which in turn produces a shift in frequency and rate of increase. Note that the excitation of the internal motion leads to a CM motion which would not have occurred if the dimer had been rigid. In that case the CM would have kept the initial oscillatory behaviour around the equilibrium position. Here, instead, the internal vibrations play a role similar to that of a heat bath and drive the CM away from the minimum with jumps across one or more potential wells.
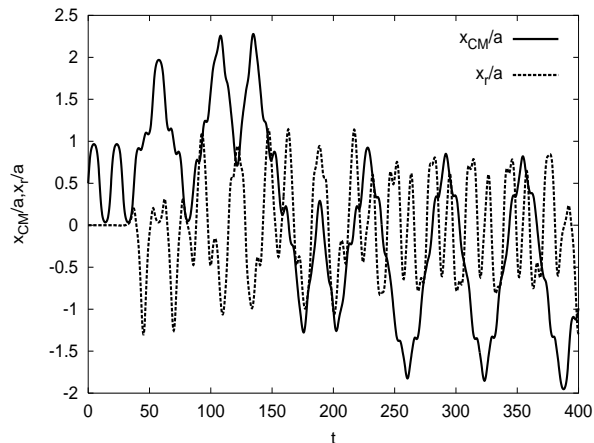

FIG. 4. Numerical simulations of Eq. (5) for $U_0 = 0.6$, $K = 0.05$ and $v_0 = 1.54$. The CM (solid line) and relative motion (dashed line), rescaled to the substrate lattice constant a, are shown.

In fact, for a non-rigid dimer, it is possible to get out of the well even if $v_0 < \sqrt{4U_0}$. This happens because if the internal motion is excited, it is possible that one particle remains in the minimum whereas the other reaches the nearest maximum. In this way the energy balance is:

$$E_{kin}^0 = \frac{1}{2}v_1^2 + \frac{1}{2}v_2^2 = 2U_0 + \frac{1}{2}K(a/2)^2 \qquad (11)$$

and if K is sufficiently small the right-hand side is smaller than $4U_0$ (we assume $v_1 = v_2 = v_0$). Thus vibrational

energy can be effective in overcoming the barrier. The resulting motion of the dimer (Fig. 4) can be characterized as chaotic, as shown later in Sect. V.

It is interesting that the chaotic motion described above occurs at velocities below and above the threshold $\sqrt{4U_0}$ for drift motion in the linearized system. This is due to a coexistence of long jumps with localized motion which persists for a certain range of initial energies, as suggested in Ref. [6]. In Fig. 5(a) we show the case where $v_0 = \sqrt{4U_0}$. At the beginning, the CM performs a step-like motion: every time it overcomes a barrier it gets stuck for a while in the next minimum before overcoming the next barrier. In this initial stage $x_r = 0$. After x_r gets excited, this step-like motion disappears. The parametric resonance which one would have expected in this case for the simplified system is not visible because of the reciprocal influence of CM and relative motion, which inhibits the increase of amplitude of x_r. Note that when the internal motion is excited almost all the energy is transferred to the vibrational modes, as it can be seen by the corresponding peaks in Fig. 5(d).
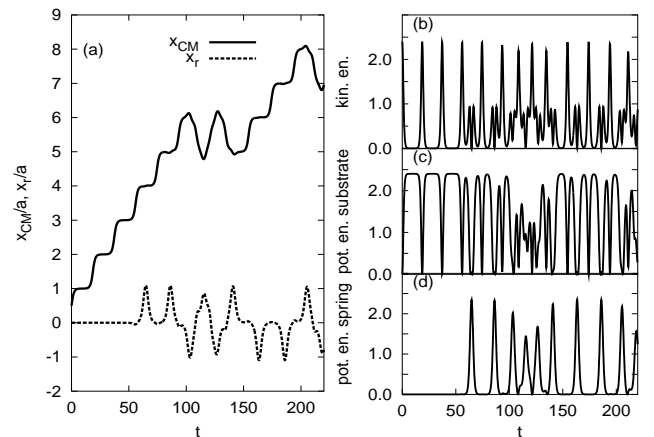

FIG. 5. Numerical simulations of Eq. (5) for $U_0 = 0.6$, $K = 0.1$ and $v_0 = \sqrt{4U_0} \simeq 1.5492$: (a) CM trajectory (solid line) and relative motion (dashed line); (b) kinetic energy; (c) substrate potential energy; (d) spring potential energy.

By further increasing the initial kinetic energy the dynamics becomes again non chaotic, and the CM performs a drift motion with constant velocity unless the conditions for parametric excitation given by Eq. (9) are met. This does not occur for the small values of K considered up to now. In fact, a dimer presents only one characteristic frequency so that conditions for parametric excitation are generally met either in the oscillatory or in the drift regime. The situation would be different for a larger molecule where different vibrational modes could be excited for different values of v_0. In Fig. 6 we show one situation for large K where the drift CM motion excites the internal motion through a parametric resonance for drift velocity twice the dimer natural stretching frequency $\omega_0 = \sqrt{2K}$. When the relative motion acquires a large amplitude, deviations from the linear behaviour of
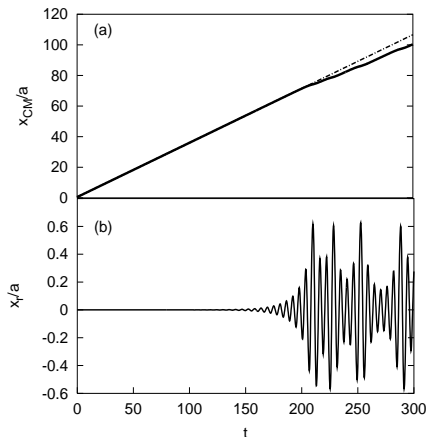
4

x_{CM} are observed.

FIG. 6. Numerical simulations of Eq. (5) for $U_0 = 0.6$, $K = 0.5$ and $v_0 = 2.5$. In (a) we show the CM motion (solid line) with a linear fit for $t < 200$ (dashed line), while the relative coordinate is plotted in (b).

In Fig. 7 we summarize for three values of K the effect of different v_0 (at fixed U_0) on the CM motion. Increasing v_0, a complex transition from oscillatory regular motion to chaotic motion and then to a drift regime can take place depending on the value of K. For $K = 0.05$ (Fig. 7(a)), resonant excitation of the internal motion occurs for $v_0 > 0.65$ as given in Fig. 1(d). Above this value, first a regime with recursive excitation of x_r, as in Fig. 3(c), takes place so that $< x_{CM} >= a/2$ and $< v_{CM} >= 0$. At $v_0 > 1.3$ the escape from the well described by Eq.(11) becomes possible. The resulting (chaotic) behaviour of x_{CM} in this regime is shown by the dashed line in Fig. 7(a) for $v_0 = 1.65$. The CM motion in this regime behaves as $< x_{CM}^2 >\simeq t^\alpha$ ($1 < \alpha < 2$) with $< v_{CM} >\simeq 0$, i.e. it is "quasi-diffusive", that is to say neither purely diffusive nor ballistic. This behavior extends up to $v_0 < 1.68$, i.e. well above the "threshold" $\sqrt{4U_0}$. Above, a drift motion $x_{CM}(t) \simeq x_0+ < v_{CM} > t$ occurs. For a larger $K = 0.3$ (Fig. 7(b)) the quasi-diffusive motion starts occurring at values of $v_0 \simeq \sqrt{4U_0}$ up to $v_0 = 2.2$, where drift motion is recovered.
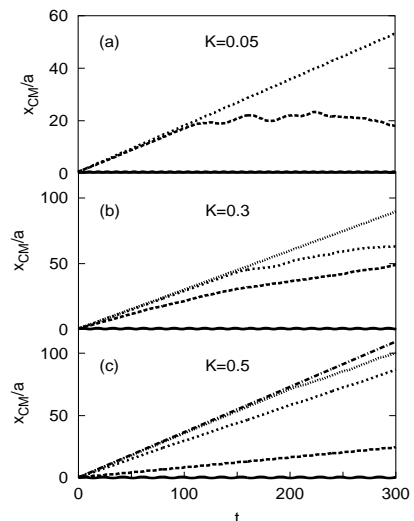

FIG. 7. Numerical simulations of Eq. (5) for $U_0 = 0.6$, three values of K and several values of v_0. The CM motion is plotted for $K = 0.05$ (a), $K = 0.3$ (b) and $K = 0.5$ (c). The different curves in each graph are obtained with different initial velocities. From bottom to top in each graph $v_0 = 0.63, 1.65, 1.68$ (a), $v_0 = 1.5, 1.85, 2.15, 2.2$ (b), $v_0 = 1.54, 1.55, 2.2, 2.5, 2.55$ (c). Note the deviation from linear behaviour in (c) for $v_0 = 2.5$ (see Fig. 6 and text).

Lastly for $K = 0.5$ (Fig. 7(c)), there is no chaotic regime. The drift motion starts at $v_0 = \sqrt{4U_0}$ and deviations only occur for a narrow range of velocities where x_r becomes parametrically excited, as shown in Fig. 6.

We may estimate from Eq. (11) the critical K value above which the internal motion is not effective in making the CM overcome the potential barrier for $v_0 < \sqrt{4U_0}$. Namely

$$2U_0 + \frac{1}{2}K_c\pi^2 = 4U_0, \qquad (12)$$

and for $U_0 = 0.6$ we find $K_c \simeq 0.35$. As a consequence for $K > K_c$ no chaotic motion is found.

B. Lennard-Jones case

Now we consider the effect of replacing the harmonic interaction (2) with a finite-range potential. As a simple choice, we take the LJ potential, given by

$$V_{LJ}(r) = 4\epsilon \left[\left(\frac{\sigma}{r}\right)^{12} - \left(\frac{\sigma}{r}\right)^6 \right] \qquad (13)$$

with $r \equiv |x_2 - x_1|$ and a cutoff at $r = 2.5\sigma$. To recover the harmonic interaction close to the minimum, we impose the equilibrium distance to be equal to the spring equilibrium length and the second derivative of V_{LJ} to be equal to the spring constant, namely:

$$\begin{cases} r_{min} & = & \sqrt[6]{2}\sigma & = & l \\ \left.\frac{d^2V_{LJ}}{dr^2}\right|_{r=r_{min}} & = & \frac{24\epsilon}{\sigma^2}\left[\frac{26}{\sqrt[3]{128}} - \frac{7}{\sqrt[3]{16}}\right] & = & K \end{cases} \qquad (14)$$

5

whence

$$\begin{cases} \sigma &=& \dfrac{l}{\sqrt[6]{2}} \\ \epsilon &=& \dfrac{Kl^2}{72} \end{cases} \qquad (15)$$

At variance with harmonic interactions, a finite-range potential allows dissociation of particles. This is clearly seen in Fig. 8, where the time behaviour of the CM and relative motion is plotted comparing the harmonic and LJ potentials.
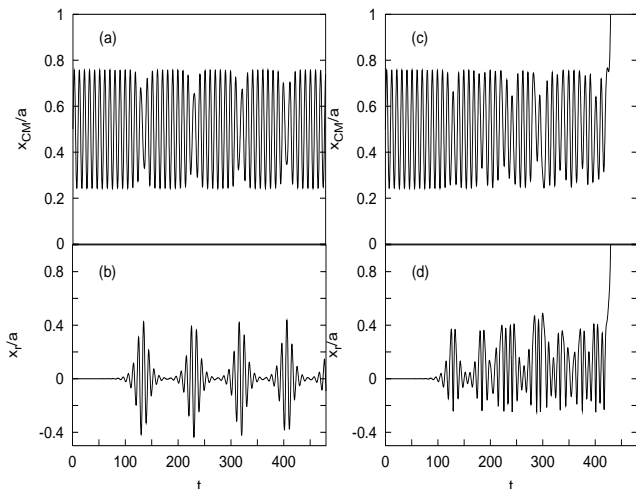

FIG. 8. Numerical simulations of the equation of motion of a dimer for harmonic (a),(b) and LJ interactions (c),(d). The CM and relative motion are shown. The parameters are $U_0 = 0.6$, $K = 0.05$, $v_0 = 1.12$ for the harmonic potential. The parameters of the LJ have been chosen according to Eq. (15): $\sigma \simeq 5.598$ and $\epsilon \simeq 0.0274$.

The CM is the same in the two cases when $x_r = 0$, i.e., at the beginning of the motion. Then, as the relative motion starts to increase, x_r given by LJ is found very similar to the harmonic x_r, but then the amplitude of the oscillations due to the LJ potential becomes larger. At $t \simeq 420$ the two particles dissociate and x_r starts to increase very fast since only one particle moves.

In Fig. 9 we show a similar process for the case where the CM performs a drift motion. We observe that the increase of amplitude of x_r occurs approximately at the same time for both harmonic and LJ interactions. As just noted above, at this point a departure from the linear behaviour of the CM takes place. While large oscillations persist in the harmonic x_r, breaking of the interparticle bond is found in the LJ case. This shows that the resonant excitation of internal vibrations could be effective in leading to dissociation of molecular bonds.
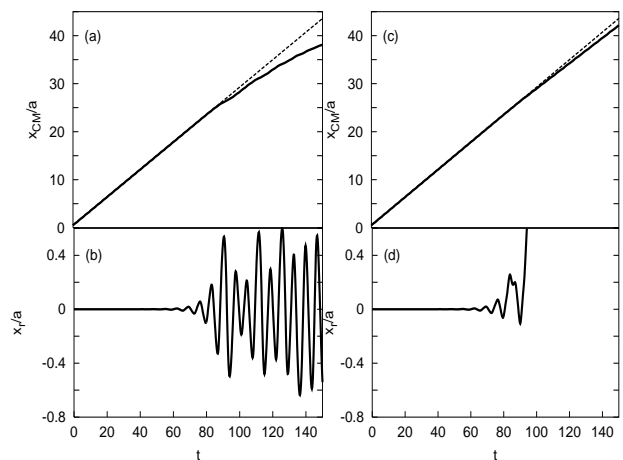

FIG. 9. Numerical simulations of the equation of motion of a dimer for harmonic (a),(b) and LJ interactions (c),(d). The CM and relative motion are shown. The dashed lines in (a) and (c) are linear fits to x_{CM} for $t < 80$. The parameters are $U_0 = 0.6$, $K = 0.4$ and $v_0 = 2.15$ for the harmonic potential. The parameters of the LJ have been chosen according to Eq. (15): $\sigma \simeq 5.598$ and $\epsilon \simeq 0.219$.

V. CHAOTIC DYNAMICS

The dynamics described in Sect. IV A shows very complex features, in spite of the simplicity of our model. The quasi-diffusive, irregular motion found for small values of K, as in Fig. 4, resembles characteristics peculiar to a chaotic regime. This is confirmed by looking at the temporal evolution of two trajectories starting at infinitesimally distant points. For example, Fig. 10 shows two long CM trajectories with initial spatial conditions differing from 10^{-6}. The behaviour of the CM is unpredictable and the trajectories diverge for the entire simulation time. This is a qualitative signature of chaotic dynamics. In order to characterize more quantitatively the chaotic motion, we have numerically computed the Lyapunov exponent, which measures the rate of divergence of nearby trajectories (see [28,29]):

$$\delta x(t) \sim \delta x(0) e^{\lambda t}, \qquad (16)$$

where $\delta x(t)$ denotes the separation between nearby trajectories and λ is the Lyapunov exponent.

In an $n-$ dimensional phase space n Lyapunov exponents can be calculated, but we limit ourselves to the computation of the maximal Lyapunov exponent λ_{max}, which is sufficient to signal the occurrence of chaos. If $\lambda_{max} > 0$ the motion is unstable and chaos may occur, while if $\lambda_{max} < 0$ we have a regular stable motion ($\lambda_{max} = 0$ corresponds to a stable quasi-periodic motion). We show λ_{max} as a function of time for a small value of K ($K = 0.05$ and $U_0 = 0.6$) in Fig. 11 for different v_0. The saturation values of the different curves give a measure of the corresponding maximal Lyapunov exponent.
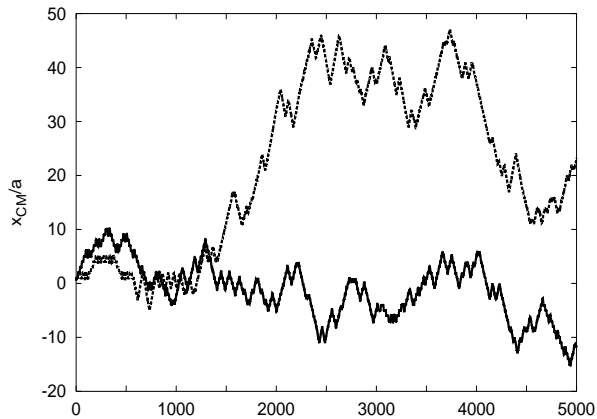
6

FIG. 10. CM motion for $U_0 = 0.6$, $K = 0.1$ and $v_0 = \sqrt{4U_0} \simeq 1.5492$, starting from different initial conditions: $x_1(0) = 0$, $x_2(0) = a$ (solid line) and $x_1(0) = 10^{-6}$, $x_2(0) = a + 10^{-6}$ (dashed line).

We note that for low values of v_0 ($v_0 = 0.63$ in the figure) $\lambda_{max} = 0$, meaning that the motion in this range is regular: x_{CM} oscillates periodically and $x_r \simeq 0$. When the internal motion starts to be excited ($0.65 \leq v_0 < 1.4$) λ_{max} jumps to a positive small value ($\lambda_{max} \simeq 0.02$), signalling that a weak chaotic dynamics is induced by the relative coordinate.
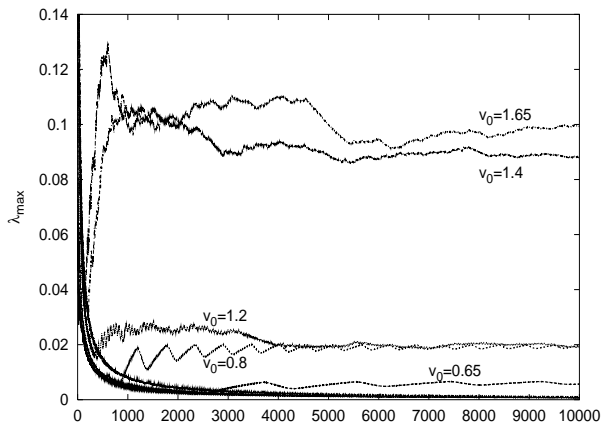

FIG. 11. Temporal behaviour of the maximal Lyapunov exponent for $U_0 = 0.6$, $K = 0.05$ and different initial velocities v_0, which are reported beside each curve, except for the two curves that saturate at zero, which correspond to $v_0 = 0.63$ and $v_0 = 1.68$.

For larger values of v_0 ($1.4 \leq v_0 < 1.68$), as the CM gets out of the minimum of the potential well and performs an irregular motion of the type shown in Fig. 4, the magnitude of λ_{max} suddenly increases of about one order of magnitude ($\lambda_{max} \simeq 0.1$), but jumps again discontinuously to zero when v_0 is high enough for the CM to perform a drift motion and $x_r \simeq 0$. In this way, we have a complex transition from non-chaotic to chaotic motion and viceversa as a function of the initial velocity. This behaviour is different from that of the double pendulum,

where the non-chaotic regime is not recovered for large initial velocities [24,25].

As a further indicator of such a dynamical behaviour we have plotted the phase space projected on the (x_{CM}, v_{CM}) plane in Fig. 12, for four different initial velocities.
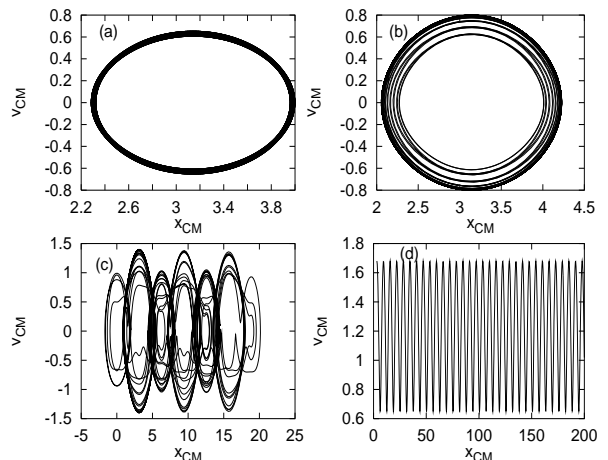

FIG. 12. Phase space plot projected on the (x_{CM}, v_{CM}) plane for $U_0 = 0.6$, $K = 0.05$ and four values of v_0: $v_0 = 0.63$ (a), $v_0 = 0.8$ (b), $v_0 = 1.4$ (c) and $v_0 = 1.68$ (d).

The phase plot in (a) is a simple closed loop corresponding to a regular oscillatory motion where $\lambda_{max} = 0$. As the initial velocity increases more complex features appear: in the weak chaotic regime (b) extra loops are present, while the phase plot in (c) becomes very much folded and irregular. The regular dynamics is restored again in (d), where there is a drift motion of the CM, with v_{CM} oscillating around the drift velocity.

Power spectrum analysis is usually considered as an additional effective method to detect chaos. We have calculated the power spectra of x_r by using a fast Fourier transform and we show them in Fig. 13 for the same values of U_0, K and v_0 as in Fig. 12. The power spectrum for the regular motion (a) is smooth and has few peaks, at $\omega_{osc}, 3\omega_{osc}, 5\omega_{osc}, ...$, i.e. the harmonics expected for a parametric oscillator. In (b) each peak broadens, developing further lateral features. For the most chaotic motion (c) the power spectrum becomes very irregular with a large number of peaks. This chaoticity disappears for higher velocities (d), where the motion is regular and the power spectrum is again smooth with a large peak at $\omega = \sqrt{2K}$ corresponding to the dimer stretching frequency.
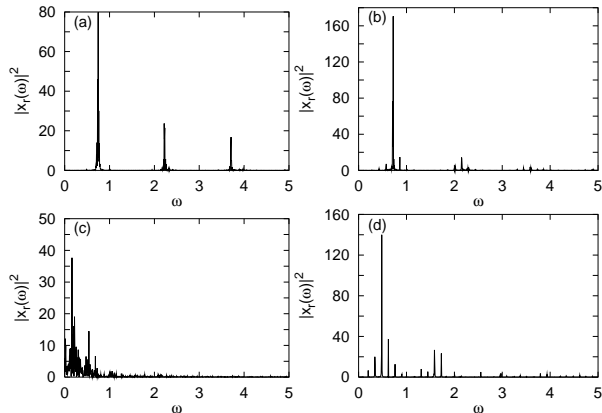
7

FIG. 13. Power spectra of the relative coordinate $|x_r(\omega)|^2$ for $U_0 = 0.6$, $K = 0.05$ and four values of v_0: $v_0 = 0.63$ (a), $v_0 = 0.8$ (b), $v_0 = 1.4$ (c) and $v_0 = 1.68$ (d).

VI. CONCLUSIONS AND DISCUSSION

In this paper, we have studied a one-dimensional model of a dimer moving on a rigid periodic substrate. We have shown how the nonlinear effects due to the substrate potential and to the interplay between the CM and relative motion can be relevant in determining the peculiar characteristics of the dimer motion. A complex dynamical behaviour is found as a function of the initial kinetic energy with the occurrence of resonant instabilities and chaotic motion. In particular, for weakly bound dimers a chaotic regime is found for a whole range of velocities between two non-chaotic phases at low and high kinetic energy. We have characterized this chaotic regime by studying the Lyapunov exponents and power spectra. Moreover, we have shown that if more realistic, finite-range interactions are considered, dimer dissociation can be induced via this mechanism by choosing appropriate initial velocities.

Although our model neglects thermal fluctuations, we can try to make some qualitative predictions concerning the effect of a finite substrate temperature, modelled by stochastic forces and a damping term, on the diffusive dynamics. The introduction of these effects could smear out all the deterministic effects. The stable periodic orbits become attracting centres via dissipation, so that the regular and chaotic motions would be only transient. On the other hand, temperature should be effective to provide energy to escape from an attractor, giving rise to a diffusive motion. Nevertheless, we expect that for small temperatures and small friction coefficients, the thermal equilibration time should be bigger than the equilibration time due to the deterministic chaotic dynamics [6]. Thus, under such circumstances, the effects explained in this paper could be significant also for real systems at finite temperature at short time scales. In particular, diffusion should be highly promoted for weakly bound dimers for which we found the chaotic features. Indeed, as reported in Ref. [9], the diffusion coefficient decreases by about an order of magnitude with respect to the non-interacting case $K = 0$, when the elastic constant is increased from $K = 0$ to $K = 0.25$, at least for small values of the damping and the temperature. Moreover, signatures of the chaotic regime can be recognized in the jump length distribution: jumps of the adsorbate over many lattice parameters are predicted by theoretical models (see for example [11,30]) and observed experimentally (see [31]). A preliminary study of the same model at $T \neq 0$ shows that the coexistence of localized and unbounded motion of the type shown in Fig. 12(c),is present up to temperatures a few times higher than the potential barrier $2U_0$. The relation between chaotic deterministic diffusion and stochastic thermal diffusion is an important topic currently under study [6,32]. This represents a connection between the behaviour of our simplified model and the one of more realistic systems. Therefore we believe that, beside their intrinsic interest, our results can be of importance to understand the dynamical behaviour of dimers moving onto real surfaces.

Note added in proof. After completion of this manuscript we have noted the recent paper A. S. Kovalev, A. I. Landau, Low Temp. Phys. **28**, 423 (2002) presenting related numerical results of diffusive dimer dynamics.

[1] J. A. Venables, G. D. T. Spiller, M. Hanbucken, Rep. Progr. Phys. **47**, 399 (1984).

[2] H. Risken, *The Fokker-Planck Equation* 2nd edn., chapter 11 (Springer, Berlin, 1989).

[3] G. L. Kellog, Surf. Sci. Rep. **21**, 1 (1994).

[4] P. J. Feibelman, Phys. Rev. Lett. **65**, 729 (1990).

[5] R. Ferrando, Phys. Rev. Lett. **76**, 4195 (1996); F. Montalenti, R. Ferrando, Phys. Rev. B **58**, 3617 (1998).

[6] R. Guantes, J. L. Vega, S. Miret-Artés, Phys. Rev. B **64**, 245415 (2001).

[7] R. Wang, K. A. Fichthorn, Phys. Rev. B **48**, 18288 (1993).

[8] O. M. Braun, Surf. Sci. **230**, 262 (1990).

[9] O. M. Braun, Phys. Rev. E **63**, 011102 (2001).

[10] F. Montalenti, R. Ferrando, Phys. Rev. Lett. **82**, 1498 (1999).

[11] F. Montalenti, R. Ferrando, Phys. Rev. B **60**, 11102 (1999).

[12] F. Montalenti, R. Ferrando, Phys. Rev. E **61**, 3411 (2000).

[13] A. Bogicevic, S. Liu, J. Jacobsen, B. Lundqvist, H. Metiu, Phys. Rev. B **57**, R9459 (1998).

[14] G. Boisvert, L. J. Lewis, Phys. Rev. B **56**, 7643 (1997).

[15] U. Kürpick, Phys. Rev. B **63**, 045409 (2001); P. J. Feibelman, Phys. Rev. B **61**, R2452 (2000); F. Montalenti, R. Ferrando. Surf. Sci. **432**, 27 (1999).

[16] A. Venkatesan, M. Lakshmanan, Phys. Rev. E **56**, 6321 (1997).

[17] S.-Y. Kim, B. Hu, Phys. Rev. E **58**, 3028 (1998); S.-Y. Kim, B. Hu, Phys. Rev. E **58**, 7231 (1998); S.-Y. Kim, Y. Kim, Phys. Rev. E **61**, 6517 (2000) .

[18] Y. Kao, C. Wang, Phys. Rev. E **48**, 2514 (1993).

[19] U. Parlitz, W. Lauterborn, Phys. Rev. A **36**, 1428 (1987).

[20] K. Murali, M. Lakshmanan, Phys. Rev. E **48**, R1624 (1993).

[21] T. Strunz, F.-J. Elmer, Phys. Rev. E **58**, 1612 (1998).

[22] B.-Y. Ou, X.-G. Zhao, S.-G. Chen, Physica B **269**, 145 (1999).

[23] S. Kocić, Lj. Ristovski, N. Burić, Chaos, Solitons and Fractals **12**, 1839 (2001) .

[24] T. Shinbrot, C. Grebogi, J. Wisdom, J. A. Yorke, Am. J. Phys. **60**, 491 (1992).

[25] R. B. Levien, S.M. Tan, Am. J. Phys. **61**, 1038 (1993).

[26] D. J. Christini, J. J. Collins, P. S. Linsay, Phys. Rev. E **54**, 4824 (1996).

[27] See for example *Berkeley Physics Course - Vol. 1 (Mechanics)*, pag. 225-227 (Mcgraw-Hill Book Company, New York, 1962).

[28] J.-P. Eckmann, D. Ruelle, Rev. Mod. Phys **57**, 617 (1985).

[29] J.-P. Eckmann , S. Oliffson Kamphorst, D. Ruelle, S. Ciliberto, Phys. Rev. A **34**, 4971 (1986).

[30] O. M. Braun, R. Ferrando, Phys. Rev. E **65**, 061107 (2002).

[31] M. Schunack, T. R. Linderoth, F. Rosei, E. Laegsgaard, I. Stensgaard, F. Besenbacher, Phys. Rev. Lett. **88**, 156102 (2002).

[32] C. Fusco, A. Fasolino, Proceedings of the EMRS Conference 2002, to be published on "Thin Solid Films"; C. Fusco, A. Fasolino, in preparation.